Developing a novel dual-injection FDG-PET imaging methodology to study the functional neuroanatomy of gait

Hilmar P. Sigurdsson [a,*], Lisa Alcock [a,b], Michael Firbank [a], Ross Wilson [a], Philip Brown [b], Ross Maxwell [a], Elizabeth Bennett [c], Nicola Pavese [a,d], David J. Brooks [a,d], Lynn Rochester [a,b]

[a] Clinical Ageing Research Unit, Translational and Clinical Research Institute, Faculty of Medical Sciences, Campus for Aging and Vitality, Newcastle University, Newcastle Upon Tyne NE4 5PL, UK
[b] National Institute for Health and Care Research (NIHR) Newcastle Biomedical Research Centre (BRC), Newcastle University and The Newcastle Upon Tyne Hospitals NHS Foundation Trust, Newcastle upon Tyne, UK
[c] North Cumbria Integrated Care NHS Foundation Trust, Carlisle, UK
[d] Department of Nuclear Medicine and PET, Institute of Clinical Medicine, Aarhus University, Denmark

ABSTRACT

Gait is an excellent indicator of physical, emotional, and mental health. Previous studies have shown that gait impairments in ageing are common, but the neural basis of these impairments are unclear. Existing methodologies are suboptimal and novel paradigms capable of capturing neural activation related to real walking are needed. In this study, we used a hybrid PET/MR system and measured glucose metabolism related to both walking and standing with a dual-injection paradigm in a single study session. For this study, 15 healthy older adults (10 females, age range: 60.5-70.7 years) with normal cognition were recruited from the community. Each participant received an intravenous injection of [^{18}F]-2-fluoro-2-deoxyglucose (FDG) before engaging in two distinct tasks, a static postural control task (standing) and a walking task. After each task, participants were imaged. To discern independent neural functions related to walking compared to standing, we applied a bespoke dose correction to remove the residual ^{18}F signal of the first scan (PET$_{STAND}$) from the second scan (PET$_{WALK}$) and proportional scaling to the global mean, cerebellum, or white matter (WM). Whole-brain differences in walking-elicited neural activity measured with FDG-PET were assessed using a one-sample t-test. In this study, we show that a dual-injection paradigm in healthy older adults is feasible with biologically valid findings. Our results with a dose correction and scaling to the global mean showed that walking, compared to standing, increased glucose consumption in the cuneus ($Z = 7.03$), the temporal gyrus ($Z = 6.91$) and the orbital frontal cortex ($Z = 6.71$). Subcortically, we observed increased glucose metabolism in the supraspinal locomotor network including the thalamus ($Z = 6.55$), cerebellar vermis and the brainstem (pedunculopontine/mesencephalic locomotor region). Exploratory analyses using proportional scaling to the cerebellum and WM returned similar findings. Here, we have established the feasibility and tolerability of a novel method capable of capturing neural activations related to actual walking and extended previous knowledge including the recruitment of brain regions involved in sensory processing. Our paradigm could be used to explore pathological alterations in various gait disorders.

1. Introduction

Gait impairment is a common feature of older age, as well as neurodegenerative conditions such as Parkinson's disease (Baltadjieva et al., 2006; Wilson et al., 2020). These changes contribute to an increased frequency of falls, negatively impacting mental health, independence, and quality of life (Axer et al., 2010; Gribbin et al., 2009). A detailed understanding of the neural networks involved in the control of

gait is still emerging. This limits the ability to develop informed interventions to tackle mobility loss and its consequences.

Imaging brain activation related to walking is commonly performed using functional MRI (fMRI). However, this is challenging due to constraints imposed by the scanner requiring the participant to lie supine and keep their head still. Recent studies have attempted to assess brain function using proxy models of gait that simulate gait movements while participants depress foot pedals (Bürki et al., 2017) or use robotic

---

assistant MR-compatible stepping devices (Jaeger et al., 2014). Others have utilised covert motor tasks that employ mental imagery or virtual reality that simulate the first-person perspective of locomotion revealing the associated brain activity (Jahn et al., 2004, 2008; la Fougère et al., 2010). These paradigms, however, may underestimate important gait components necessary for real-world mobility such as vestibular input, visual processing, and sensory-motor integration. Moreover, motor imagery tasks can be challenging and burdensome for elderly participants and patient populations alike whose vividness of mental imagery may be compromised (Personnier et al., 2010; Pickett et al., 2012) further highlighting the need for new methodologies capable of capturing the whole process.

[^{18}F]-2-fluoro-2-deoxyglucose positron emission tomography (FDG-PET) can be used to study neural activity related to gait and postural control (Sigurdsson et al., 2022). Glucose is the main metabolic substrate of the brain and FDG-PET, as a marker of hexokinase activity, allows the measurement of the brain's energy demands. FDG enters cells and becomes phosphorylated by the rate limiting enzyme hexokinase forming FDG-6-P, but unlike glucose, it cannot be further metabolised becoming irreversibly trapped and accumulating in brain cells during PET (Reivich et al., 1979). FDG can be administered intravenously prior to walking, and the associated gait metabolism can subsequently be measured while subjects are lying supine at rest (la Fougère et al., 2010). Current paradigms, however, require two FDG-PET measures to be acquired in separate study sessions. This becomes a particularly important limiting factor when performing brain activation studies as people's state of mind and motor function can change from day to day. The burden of multiple sessions can also be difficult for many.

For the current pilot study, we used a repeated method of intravenous FDG administration to allow differentiation of gait-related brain activity from that of maintaining a standing posture in 15 healthy older adults in a single study session. The primary aim of this project was to demonstrate the feasibility and proof of concept of a novel, single-session, hybrid FDG-PET methodology for studying regional brain metabolism during real-time gait using dynamic functional imaging of brain glucose utilisation with FDG-PET. Our objective was to develop a novel, dynamic and comprehensive framework that can elucidate the neural activity required for walking that could ultimately support the development of novel interventions.

2. Materials and methods

2.1. Participants

A total of 15 healthy older community-dwelling adults (10 females, mean age: 65.0 ± 2.9, age range: 60.5-70.7 years) capable of standing and walking independently for a minimum of five minutes without rest were recruited between November 2019 – October 2020. Participants were excluded if they had a diagnosis of diabetes mellitus or fasting blood glucose levels of > 7 mM/L, had evidence of cognitive impairment when assessed using the mini-mental state exam (Folstein et al., 1975), had a history of severe orthopaedic pathology severely affecting gait, history of falls, contraindications for PET/MRI and FDG administration (e.g., self-reported claustrophobia, renal impairment), unable to comply with the testing protocol, and currently participating in another conflicting research study. All participants provided written informed consent. The study received ethical approval from the HRA (East Midlands – Nottingham 1 Research Ethics Committee) and Health and Care Research Wales (Ref: 19/EM/0212) and approval from the Radioactive Substance Advisory Committee (ARSAC, Ref ID: 439).

2.2. Study protocol

The study protocol timeline is depicted in Fig. 1. All participants visited the Centre for In Vivo Imaging (CIVI), Newcastle University for a single study session. We recorded participant demographics and anthropometrics. Becks Depression Inventory was used to record current mood, pessimism, and irritability (Beck et al., 1961). Participants were asked to fast for at least 6 h before the study session. Blood glucose was measured using a pinprick to confirm a fasting blood glucose of 4–7 mmol/l at the start of the session. Then, participants received an intravenous injection of 100 MBq of the FDG tracer through a cannula over 20 seconds. This was immediately followed by a 15-min upright standing task (participants were asked to focus on a fixation cross placed approximately 3 m away to reduce head movements and visual inputs; carried out in 5-min blocks with 1-min rest [sitting] in between each block). The bed was detached from the scanner and placed next to participants in the adjacent room to minimize movement between experimental trials (standing and walking) and scanning protocol. Participants then had a 16-min PET/MR scan while resting supine 30-min after receiving the first FDG injection. Following a short break, participants' blood glucose levels were measured again followed by another FDG intravenous injection. Participants then completed a 15-min standardised walking task (walk at a comfortable pace, anticlockwise around an 8-m track; 5-min blocks with 1-min rest [sitting]) followed by a second 16-min resting PET/MR scan (30-min post second FDG injection). The order of tasks was fixed, and standing was always followed by walking. For both conditions, small lightweight body-worn monitors were attached to measure movement and wireless surface EMG sensors were attached over key leg muscles to measure muscle activity. All sensors were removed before and re-attached after the first PET/MR scan. Here we provide basic gait characteristics as descriptors of functional mobility computed using bespoke algorithms from our group (Del Din et al., 2016).

2.3. PET/MR imaging acquisition

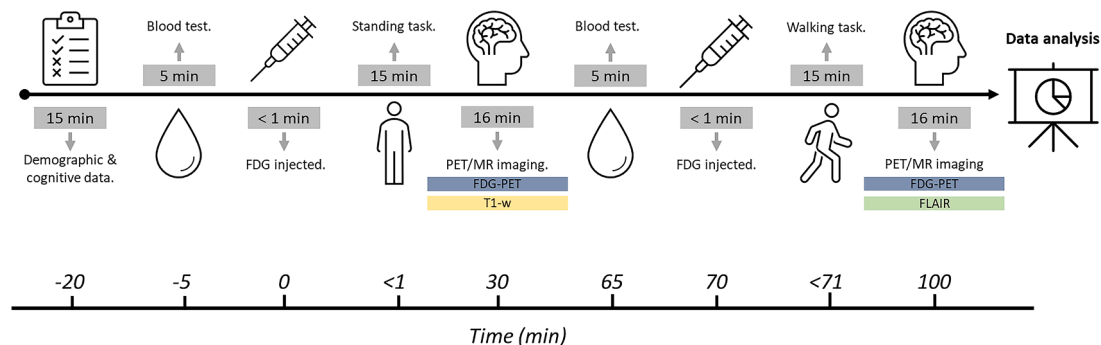All participants were imaged with a GE hybrid PET/MR 3T Signa

Fig. 1. Study visit timeline. Time in grey-filled boxes indicate the duration of the procedure/task. Timeline at the bottom of the figure indicates the elapsed time from the start of the first injection (Time 0 min) to the start of the second scan (Time 100 min) in minutes. Each event is indicated by the approximate start time relative to the first FDG injection. Abbreviations: FDG - [^{18}F]-2-fluoro-2-deoxyglucose, T1-w – T1-weighted MRI, FLAIR - fluid attenuated inversion recovery.

scanner (GE Healthcare, Waukesha, WI, USA) equipped with a 32-channel head coil (Nova Medical, Wilmington, MA, USA). Foam padding was added between the participants' head and the head coil. FDG-PET was acquired twice (after standing and walking) in 3D list mode (matrix size – 192×192, voxel size – 1.56×1.56×2.78 mm) with decay, attenuation, scatter, and dead-time corrections. FDG-PET scans were 'static' scans in that we did not attempt to assess the kinetic properties of tracer distribution and instead treated the integrated activity distribution as a snapshot across the 16-min period acquired 30 min post uptake as unchanging. We reconstructed each 16-min acquisition as a series of short 2-min frames to allow inter-scan head motion correction. We used standard PET reconstruction settings – time-of-flight mode with 8 iterations, 28 subsets and a 3 mm filter. Optimisation of reconstruction parameters was additionally carried out. We computed a parametric image of FDG activity distribution using all coincident 511 keV emissions detected in this period.

A 3D T1-weighted (T1-w) magnetization-prepared rapid acquisition gradient-echo sequence (MPRAGE, parallel acceleration factor = 2, matrix size – 256 × 256, voxel size – 1 mm isotropic, TR/TE/TI – 7/3/900 ms, flip angle – 8°) was also run concurrently with FDG-PET following the standing task (PET$_{STAND}$). Then, fast fluid-attenuated inversion recovery (FLAIR, TR/TE/TI – 13000/133/2759 ms) was run concurrently with the FDG-PET scan following the walking task (PET$_{WALK}$). FLAIR scans were reviewed to assess the density of white matter hyperintensities (WMH) as a marker of vascular disease in participants. Multi-shell diffusion weighted images and multi-echo resting-state fMRI images were acquired concurrently with PET$_{STAND}$ and PET$_{WALK}$, respectively.

2.4. Imaging data postprocessing

FDG-PET and T1-w data were analysed using SPM12 (v7771; Wellcome Trust Centre for Neuroimaging, http://www.fil.ion.ucl.ac.uk) running on MATLAB (r2018a; The MathWorks Inc., Natick, MA, USA). All Digital Imaging and Communications in Medicine (DICOM) images were anonymized and converted to compressed Neuroimaging Informatics Technology Initiative (NifTI) format using the dcm2niix tool (https://github.com/rordenlab/dcm2niix).

2.4.1. Structural MRI

We followed the Mayo Clinic Adult Lifespan Template (MCALT) segmentation pipeline suitable for older adults (Schwarz et al., 2018) but replaced the MCALT-specific tissue prior with those from SPM12. First, the T1-w images were re-oriented to align with the AC-PC line in MNI space using the Automatic Registration Toolbox (https://www.nitrc.org/projects/art). Then, in SPM12 the T1-w images were segmented into probabilistic grey matter (GM), white matter (WM) and CSF compartments. Modulated GM probability maps were spatially warped into standard stereotactic MNI space, with both forward and inverse deformations stored, as well as the bias-field corrected image. Warped images had a 2 mm isotropic voxel resolution. The probabilistic GM maps in native space were smoothed to 6 mm FWHM (full-width at half-maximum) to resemble the smoothed FDG-PET images. The total intracranial volume (TIV) as the sum of the GM, WM and CSF was recorded (in ml).

2.4.2. FLAIR

The T2-FLAIR images were processed using SPM12's extension Lesion Segmentation Toolbox (LST) (Schmidt et al., 2012). The LST employs a lesion growth algorithm and an iteration process to detect outliers in tissue classes and label these as WMHs. For our study, we applied this method to the T2-FLAIR images (in native space) with the default parameters. Since SPM12 tends to misclassify WMHs as grey matter during the segmentation process (Levy-Cooperman et al., 2008), WMHs were removed from GM maps and reclassified as WM. For each participant, we computed WMH volumes as the log of the ratio of WMH

to total brain volume and number of lesions (see Table 1).

2.4.3. FDG-PET

Brain FDG uptake reflecting the cerebral metabolic rate of glucose was quantified using the following steps in SPM12. First, PET$_{STAND}$ and PET$_{WALK}$ images were aligned with registration to halfway space (parameters: quality = 0.9; separation = 4; FWHM smoothing = 7 mm; interpolation = 2nd Bspline) creating a mean, resliced image. This ensured that both images underwent identical processing. Second, the mean image was co-registered to the smoothed probabilistic (corrected) GM map and the affine transformation matrix was applied to both PET$_{STAND}$ and PET$_{WALK}$ images. Third, we computed a contrast image, subtracting any activity in the PET$_{STAND}$ image from the PET$_{WALK}$ image. This calculation also accounted for FDG which would remain in the system during PET$_{WALK}$ from the initial PET$_{STAND}$ due to the short duration between scans (average time elapsed = 72.3 ± 9.3 min). That is, the PET$_{WALK}$ image includes a contribution from both the first and second injections of FDG. Since radioactive distribution at the time of the first image acquisition (PET$_{STAND}$) is known, we can remove residual activity by radioactive decay correcting this first acquisition for the delay between acquisitions 1 and 2, subtract from acquisition 2 (PET$_{WALK}$) and then compute the corrected PET$_{WALK}$ as shown in Eq. (1).

$$\text{Corrected } PET_{WALK} = PET_{WALK} - (f_0 \cdot PET_{STAND}) \tag{1}$$

Equation 1. Dose correction, correcting the PET$_{WALK}$ image for residual FDG from the standing period.

Where f_0 is the decay factor (see Eq. (4)) for the time between the first and second scan. The standardised uptake is the measured uptake divided by time delay (between injection and scan) corrected for injected dose (ID) as demonstrated in Eq. (2).

$$SU_{STAND} = \frac{PET_{STAND}}{f_1 \cdot ID_1}; \quad SU_{WALK} = \frac{PET_{WALK} - (f_0 \cdot PET_{STAND})}{f_2 \cdot ID_2} \tag{2}$$

Equation 2. Standardised uptake (SU) defined for PET$_{STAND}$ and PET$_{WALK}$ scans.

Where f_1 and f_2 are the decay corrections (Eq. (4)) for the time between each injection and the associated scan. The change in standardised uptake between walking and standing, for each participant, then becomes:

$$PET_{CONTRAST} = \frac{PET_{WALK} - (f_0 \cdot PET_{STAND})}{f_2 \cdot ID_2} - \frac{PET_{STAND}}{f_1 \cdot ID_1} \tag{3}$$

Equation 3. Dose correction.

Table 1
Demographic data for the sample ($n = 15$).

Variable (unit or maximum score)	Value
Demographics	
Age (years)	65.0 ± 2.90
Sex (F/M)	66 % females (10/5)
Years in education	13.73 ± 2.81
BMI (kg/m^2)	26.66 ± 3.66
Clinical scores	
MMSE (score/30)	29.6 ± 0.63
BDI (score/63)	3.87 ± 2.90
Blood glucose level$_{STAND}$ [range]	5.36 ± 0.64 [4 – 6.4]
Blood glucose level$_{WALK}$ [range]	5.11 ± 0.66 [4.4 – 6.5]
MRI data	
MBq/Kg	1.42 ± 0.22
TIV (ml)	1502.65 ± 200.70
Total WMH volume (ml)	2.61 ± 3.43
WMH-number	11.40 ± 6.56
Gait characteristics	
Mean step velocity (m/s)	1.44 ± 0.32
Mean step length (m)	0.78 ± 0.15

Data are presented as mean ± SD. Abbreviations. MMSE – mini-mental state exam, BDI – Becks depression inventory, MBq – megabecquerel, m/s – meters per second, m – meters, TIV – total intracranial volume, WMH – white matter hyperintensities.

Where,

$$f = \exp\left(-\ln(2)\cdot\frac{T}{FDG_{t1/2}}\right) \qquad (4)$$

Equation 4. Decay correction.

$FDG_{t1/2}$ has a half-life of 109.8 min. For f_0, T (time) is the elapsed time between the first (stand) and second (walk) scans in minutes. For f_1, T is the elapsed time between the first dose and the start of the first scan. For f_2, T is the elapsed time between the second dose and the start of the second scan. ID_1 and ID_2 are the radiopharmaceutical doses administered to the participant (in MBq). This approach was validated using phantom pilot data. A polypropylene bottle was filled with 2 L of water and 7.44 MBq of FDG was added followed by a PET scan 11 min later. A second dose of FDG (7.26 MBq) was then added to the same bottle 54 min after the first addition and scanned 17 min later (60 min after the first scan). Images were reconstructed as per human participant scans but without attenuation correction. Scans were aligned together using registration tools in SPM12 and Equation 3 was applied to calculate the change in uptake after correcting for residual uptake from scan1 on scan2 and decay of activity. To compare against the original images, we multiplied the calculated image by the average dose, to determine the difference in counts rather than standardised uptake. Fig. 2 shows the images and a line profile through the bottle.

The dose correction proposed above (Eq. (3) applied to co-registered PET$_{STAND}$ and PET$_{WALK}$ images) corrects the FDG-PET data within participants but the calculated PET$_{WALK}$-PET$_{STAND}$ difference may still need to be corrected for overall brain uptake (ratio normalisation) to compare between participants (Fox et al., 1988). With no current consensus available (Borghammer, 2012), we used proportional scaling using the global mean (Gx) as the average cerebral uptake from both images (following co-registration of the two FDG-PET images and to GM map), average uptake within the cerebellum (Cbl, as defined by the Hammers atlas, Hammers et al., 2003), and white matter within the central semiovale (WM) as references. WM has previously been suggested to be a

relatively unbiased reference region in ageing studies (Borghammer et al., 2008). All normalisation was done in native space using non-blurred images.

Contrast images were warped to standard MNI space using the forward deformation fields from the segmentation step and smoothed using a 6 mm Gaussian kernel at FWHM. We did not correct the FDG-PET data for any partial volume effects (PVE). Since the primary focus is on the contrast between FDG uptake during walking and standing, and the same structural image was used for this intra-subject analysis, PVE correction would have little effect on and add noise to the subsequent statistical analysis.

3. Statistical analysis

3.1. Univariate voxelwise comparison

We used a paired samples t-test for comparison of resting blood glucose levels and time interval (in minutes) between infusion of FDG with the statistical threshold set at $p < 0.05$. We used a one-sample t-test in SPM12, with an explicit binary grey matter and brainstem mask, to locate brain regions with significantly greater activity during walking relative to standing (PET$_{WALK}$ > PET$_{STAND}$). We applied a stringent voxelwise Family-Wise error (FWE) correction of $p < 0.005$ and a cluster extent threshold (k) of > 50 contiguous voxels. This stringent multiple-testing correction removes any spurious clusters reducing the likelihood of a Type I error, whereas a relatively low cluster threshold allows the detection of small sub-cortical regions. Significant clusters were labelled according to the AAL v3.1 atlas (Rolls et al., 2020).

4. Results

4.1. Group characteristics

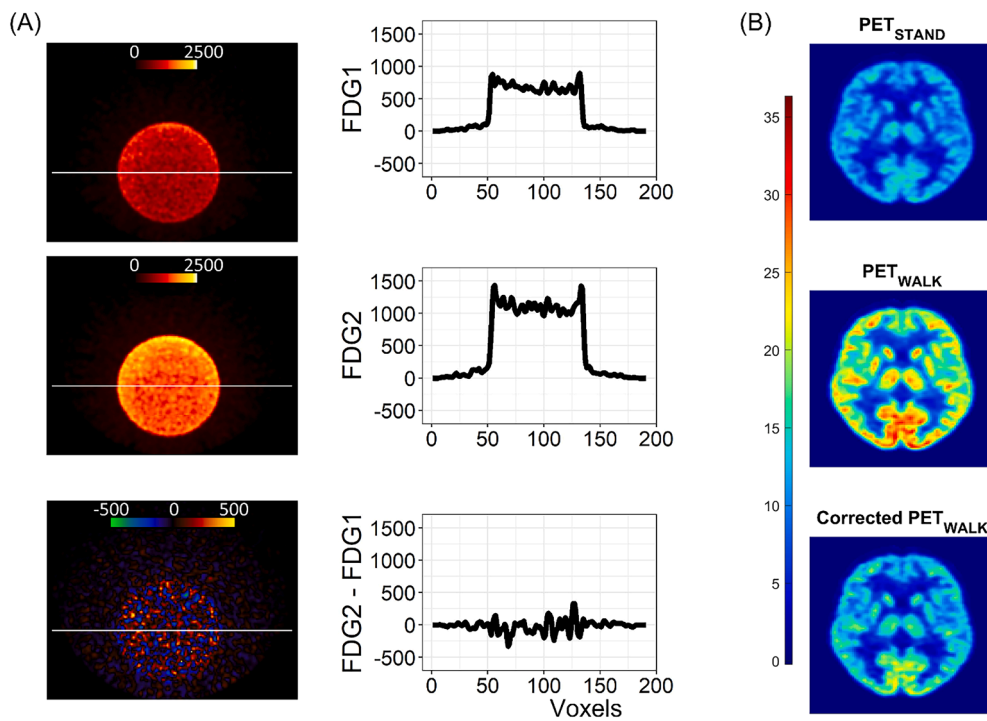All participants completed the study protocol and there were no

Fig. 2. Data analysis validation. Panel A: Image and line profile through the bottle on scans 1 (top) and 2 (middle), and the difference image (bottom) calculated according to Eq. (3). Panel B: Data from a representative participant showing the effect of the dose correction on the PET$_{WALK}$ image using Eq. (1) when applied to co-registered images in native subject space. The images were then warped to standard MNI space Top – PET$_{STAND}$, middle – uncorrected PET$_{WALK}$, bottom – corrected PET$_{WALK}$. The colorbar shows image intensity across the three images.

adverse events/ reactions. Participant characteristics are summarised in Table 1. All participants were cognitively intact with no history of neurological disorders and reported being active, taking regular walks. Resting blood glucose levels from participants before the two tasks were all within our current criteria for study inclusion (4–7 mM/l). The statistical comparison showed a non-significant difference between glucose levels measured before standing and walking ($t(14) = 1.94$, $p = 0.073$). On average, 30.33 ± 0.72 min and 32.07 ± 4.43 min elapsed between the injection of FDG and the start of PET for standing and walking conditions, respectively. Again, this was not statistically different ($t(14) = 1.46$, $p = 0.15$). Visual inspection of the imaging data revealed the data to be of excellent quality with no distortions or artefacts and no images were excluded. Further inspection of structural MRI data and FLAIR scans revealed no abnormally high volume or count of WMHs in any participant.

4.2. Neural substrates of walking

The voxel-wise analysis of the dose-corrected contrast images (using Eq. (3)) and following proportional scaling to the average global mean (Gx), elicited clusters of greater activity during walking in a canonical set of locomotor brain regions (Table 2, Fig. 3).

The highest statistical significance was within the right cuneus ($Z = 7.03$) followed by the left mid-temporal gyrus ($Z = 6.91$) and the medial orbital frontal cortex ($Z = 6.71$). We also saw increased glucose metabolism in the inferior, middle, and superior frontal cortex bilaterally, bilateral inferior, middle and superior temporal lobe that extended further to include the right posterior parietal operculum (OP2) and parts of the anterior subcentral gyrus (i.e., parieto-insular vestibular cortex), bilateral postcentral and left precentral gyri extending to include area 1/2/3 of the lower limb region and trunk within the paracentral lobule, the right mid (motor) cingulate cortex, and occipital lobe including the lingual gyrus. Subcortically, we observed increased glucose utilisation in the bilateral putamen and in a large cluster with the peak located in the right intralaminar thalamus (MNI: 8, -22, 0). This large cluster with 1801 voxels also encompassed the substantia nigra pars compacta, the red nucleus, and further regions of the thalamus, including the pulvinar, and the mediodorsal and ventral posterolateral nuclei, in both hemispheres. Further caudally, we found increased metabolism in discrete regions of the supraspinal locomotor network including the cerebellar vermis IV-V encompassing the fastigial nucleus (FN) and cerebellar locomotor region (CLR), as well as bilateral increases in the midbrain that most likely includes the midbrain locomotor region (MLR).

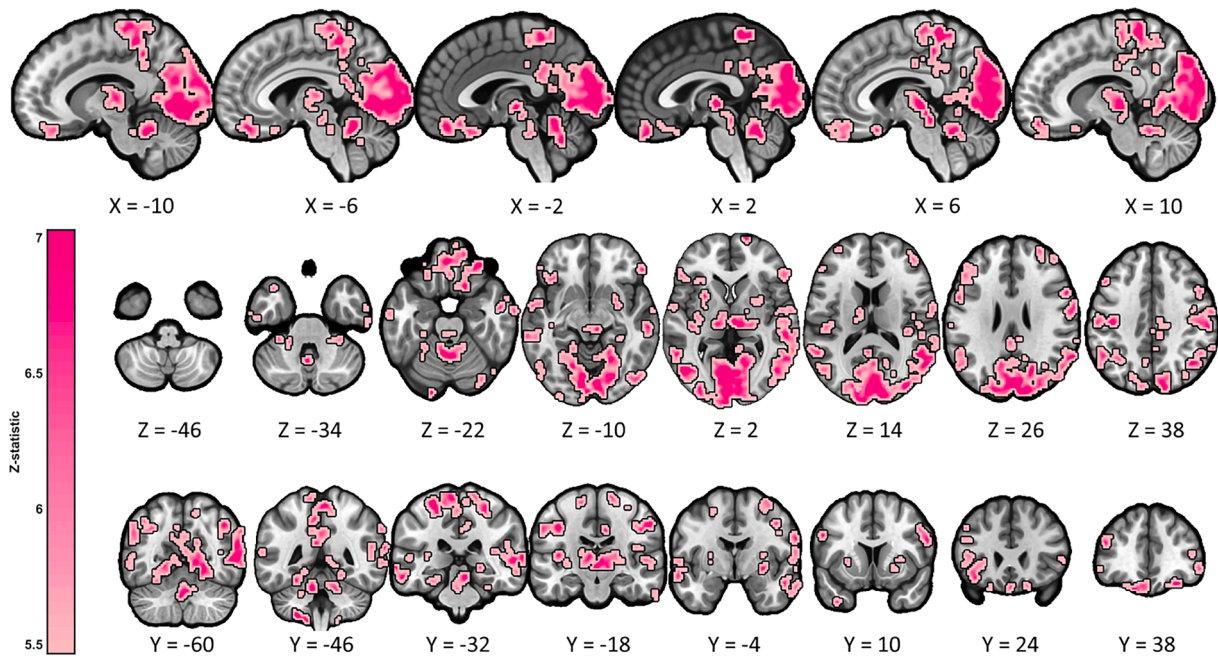Looking at the reverse contrast ($PET_{STAND} > PET_{WALK}$) did not show

Table 2

Anatomical labelling of clusters according to the AAL3.1 atlas demonstrating greater glucose metabolism during walking relative to standing following proportional scaling using the global mean (p-FWE < 0.005, $k > 50$ voxels).

Cluster	Label	Side	% of cluster	#Voxels	Z-stat	X	MNI Y	Z
1	Cuneus	R	53.66	16020	7.03	4	-82	32
	Postcentral	R	50.41		6.80	12	-36	64
2	Temporal Mid	L	71.54	1276	6.91	-48	-66	2
	Occipital Mid	L	51.22		6.19	-38	-68	6
3	OFC med	L	21.14	1005	6.71	-14	44	-28
	OFC ant	R	64.23		6.35	30	40	-20
4	Cerebellum 8	L	94.31	82	6.66	-26	-44	-52
	Cerebellum 9	L	32.52		6.21	-18	-46	-58
5	Thalamus IL	R	25.20	1801	6.55	8	-22	0
	Vermis 4-5	R	60.98		6.52	2	-54	-22
6	Cerebellum 8	R	30.89	55	6.32	16	-46	-60
7	Postcentral	L	78.86	303	6.29	-40	-20	38
	Postcentral	L	86.99		6.14	-38	-26	44
8	Cerebellum Crus1	L	45.53	84	6.27	-18	-90	-20
	Lingual	L	39.84		5.80	-22	-98	-14
9	Frontal Inf Orb 2	R	82.11	326	6.21	52	34	-6
	Frontal Mid 2	R	95.12		6.02	42	42	30
10	Frontal Mid 2	L	78.86	321	6.20	-48	22	36
	Precentral	L	81.30		6.12	-54	8	30
11	Frontal Inf Oper	R	79.67	169	6.18	52	14	32
	Frontal Inf Oper	R	82.93		6.04	56	12	24
12	Heschl gyrus	L	38.21	317	6.13	-32	-28	8
	Heschl gyrus	L	54.47		5.99	-42	-20	8
13	Temporal Inf	L	48.78	54	6.11	-38	12	-38
14	Temporal Mid	L	99.19	196	6.10	-66	-32	-4
	Temporal Mid	L	82.11		6.07	-60	-30	-14
15	Frontal Sup 2	L	24.39	79	6.09	-26	0	46
	Precentral	L	49.59		5.71	-26	-10	54
16	Frontal Sup 2	L	92.68	75	6.06	-22	64	10
	Frontal Mid 2	L	87.80		5.76	-32	54	12
17	Frontal Inf Tri	L	61.79	288	6.06	-50	28	-2
	OFC post	L	56.10		5.99	-38	24	-14
18	Frontal Mid 2	R	66.67	81	6.04	28	52	28
	Frontal Sup 2	R	99.19		5.68	22	54	20
19	Putamen	R	51.22	226	6.03	28	-4	-4
	Putamen	R	71.54		5.91	26	4	-6
20	Cingulate Mid	R	78.05	52	6.02	8	-18	34
	Cingulate Mid	R	34.15		5.69	16	-22	38
21	Frontal Sup 2	R	67.48	52	6.01	16	66	2
22	Putamen	L	95.12	95	5.99	-26	6	0
	Putamen	L	56.10		5.79	-26	-6	12
23	Temporal Mid	L	91.87	287	5.97	-58	-8	-14
	Temporal Inf	L	82.11		5.87	-54	-14	-28

Notes: R – Right hemisphere, L – Left hemisphere. % of cluster indicates the percent of cluster's voxels belonging to the specific label.

Fig. 3. Z statistical map (thresholded at *p*-FWE < .005 and *k* > 50 voxels) following proportional scaling using the global mean projected onto a standard template in MNI space showing greater glucose metabolism during walking relative to standing. Top panel – sagittal view, middle panel – axial view, bottom panel – coronal view. Numbers indicate MNI coordinates. Figure created using the CanlabCore tools (https://github.com/canlab/CanlabCore).

any significant differences in any region of the brain when corrected for multiple comparisons.

Interrogating the SPMs when proportional scaling of the data to the cerebellum or white matter (centrum semiovale) led to similar results. Fig. 4 depicts the intersection of the three correction methods. Visually, increased glucose metabolism was relatively more evident following scaling to the global mean of GM. Again, the opposite contrast returned null findings.

Fig. 5 demonstrates the impact of different reference regions on average Z-values from randomly selected ROIs. In all ROIs, with the exception of the cerebellum (CLR region), scaling to the global mean increases the statistical outcome.

Given the complexity and uncertainty in the use of proportional scaling and which reference region to use, we were curious to see how our results without this correction would compare to when such a correction is applied. Using our very stringent correction for multiple
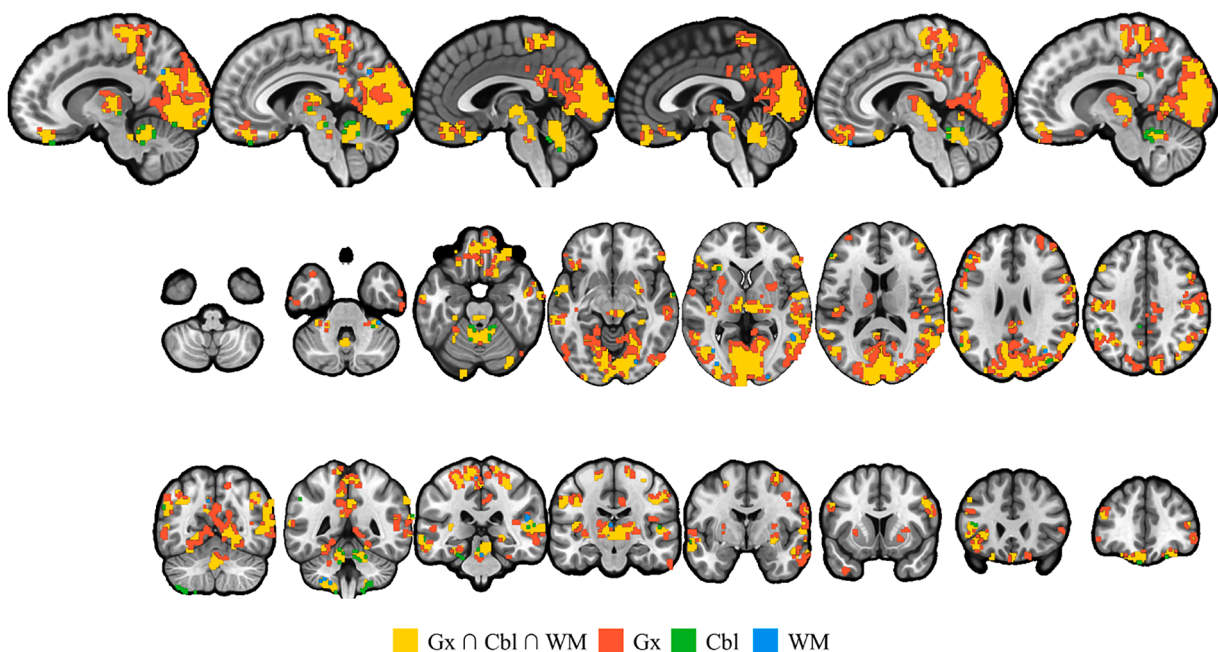

🟨 Gx ∩ Cbl ∩ WM 🟧 Gx 🟩 Cbl 🟦 WM

Fig. 4. Binarised Z statistical maps (thresholded at *p*-FWE < .005 and *k* > 50 voxels) following proportional scaling using the global mean (Gx - red), cerebellum (Cbl - green) and white matter (WM - blue) projected onto a standard template in MNI space showing greater glucose metabolism during walking relative to standing. Yellow represents the overlap of all three correction methods. Top panel – sagittal view, middle panel – axial view, bottom panel – coronal view. Figure created using the CanlabCore tools (https://github.com/canlab/CanlabCore).
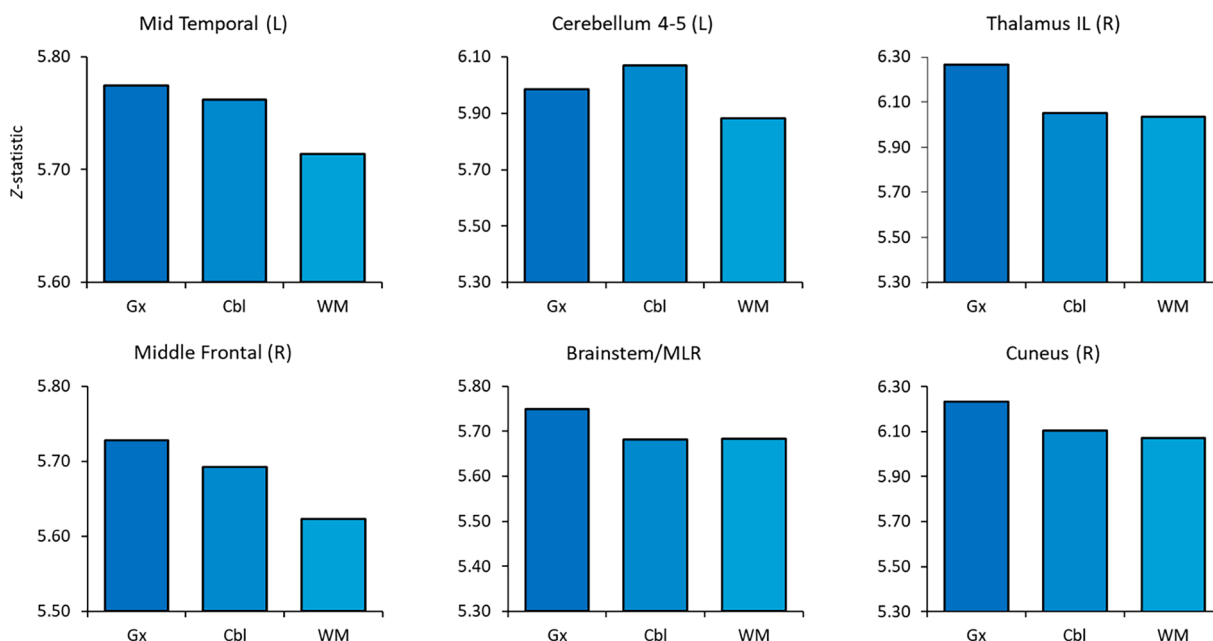
Fig. 5. Average Z-values (Y-axis) plotted for each reference region used for proportional scaling from randomly selected ROIs. Abbreviations: Gx – global scaling, Cbl – scaling to the cerebellum, WM – scaling to white matter, IL – intralaminar thalamus region, L – left, R – right.

comparisons at *p-FWE* < 0.005 showed dispersed and weak, albeit significant, findings. Relaxing the correction to *p-FWE* < 0.01 provided similar results to when the data were proportionally scaled. The results of this analysis are illustrated in Fig. 6 and anatomical labels are detailed in Table S1 in supplementary material.

5. Discussion

The primary aim of this study was to demonstrate the proof-of-concept of a novel hybrid FDG-PET methodology for studying the

functional neuroanatomy of gait in a sample of healthy older adults. The major findings of our study showed that our novel paradigm was successfully delivered demonstrating it is a feasible method to study real-time gait. Furthermore, the protocol was safe and well tolerated. We have, therefore, established the capability of this methodology to identify changes in brain glucose utilisation following two motor tasks in a single study session, substantially reducing participant burden incurred with repeated study visits. We also developed a bespoke dose correction and with this provided a clear method for measuring the neural activity related to walking in real time while accounting for the
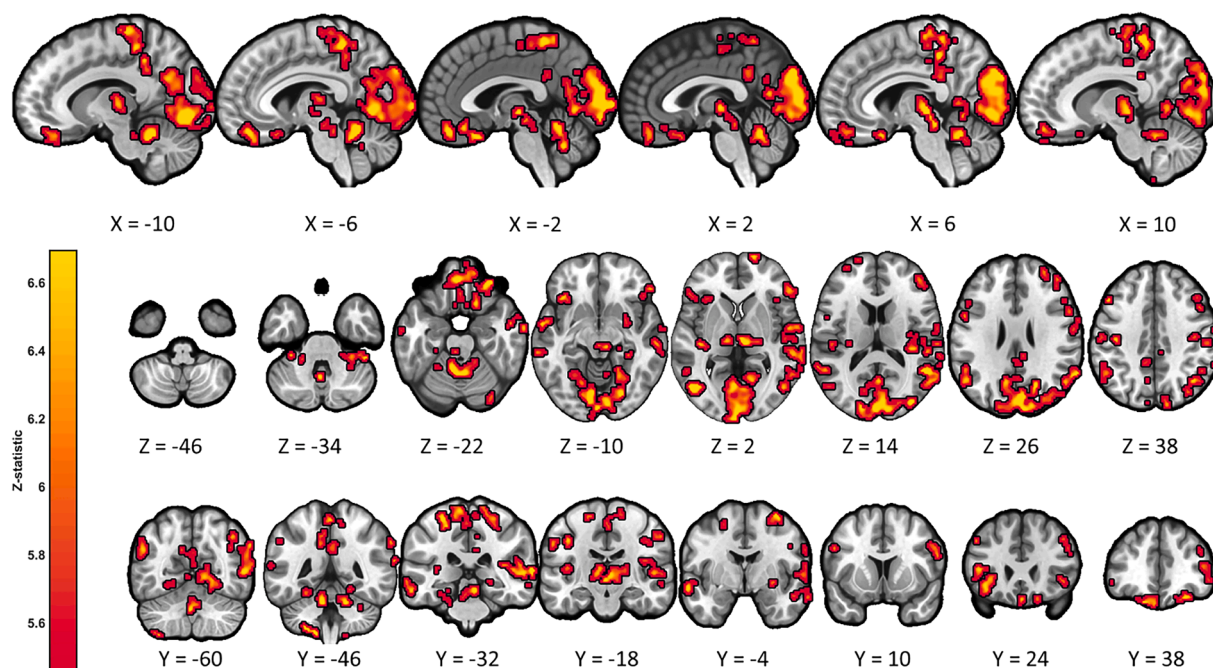

Fig. 6. Z statistical map (thresholded at *p*-FWE < .01 and *k* > 50 voxels) without proportional scaling projected onto a standard template in MNI space showing greater glucose metabolism during walking relative to standing. Top panel – sagittal view, middle panel – axial view, bottom panel – coronal view. Numbers indicate MNI coordinates. Figure is created using the CanlabCore tools (https://github.com/canlab/CanlabCore).

activity required for upright posture (static balance). Our approach revealed increased glucose metabolism in the supraspinal locomotor network including the MLR, CLR, and thalamus in addition to discrete supratentorial brain areas critical for higher-order cognitive and multi-sensory function, thereby both replicating and extending previous findings.

5.1. On the development of a multi-modal neuroimaging paradigm to study gait

Previous studies aiming to map the neural activity of walking have relied on challenging mental imagery tasks (Jahn, Deutschlander, et al., 2008; Jahn et al., 2004; la Fougère et al., 2010). These studies have provided important information about the neural substrates of walking built on the premise that imagination of an action recruits brain regions involved in actual motor planning, preparation, and performance (Hétu et al., 2013; Taube et al., 2015). However, these tasks require considerable participant co-operation which is difficult to assess and may be problematic for older adults and patient populations (Personnier et al., 2010; Pickett et al., 2012). These paradigms most likely underestimate important gait components such as proprioception, sensorimotor and visuomotor integration, and vestibular function (Hamacher et al., 2015).

In our investigation, we employed a fully integrated PET/MR system. The synergy of precision anatomy, achieved with the concurrent acquisition of anatomical MR scans alongside FDG-PET scans, played a pivotal role in fulfilling the study objectives. The high-resolution anatomical images are instrumental in precisely localizing metabolic changes observed in PET images. The selection of a hybrid PET/MR system was deliberate. While PET/CT is considered superior in clinical imaging due to rapid sequences and offers simplified attenuation correction, the superior soft tissue contrast of MRI and with that the ability to delineate intricate neural structures were important to our investigation (von Schulthess & Schlemmer, 2009). Additionally, PET/MR offers the added benefit of reduced ionizing radiation exposure (von Schulthess & Schlemmer, 2009). This is significant in multi-scan studies aligning with ethical considerations regarding participant safety thus outweighing the benefits of rapid imaging of PET/CT. Regardless of systems, we believe that our PET image subtraction methodology would work equally well with PET/CT as it does with PET/MRI.

In comparison to imaging techniques other than PET/CT, FDG-PET employed in this study offers unique advantages in capturing localized brain activity during naturalistic walking unlike fMRI, which is limited to the observation of virtual walking due to its static imaging nature. Nonetheless, PET has a poor temporal resolution (e.g., in our case we are observing the average glucose metabolism over the complete walking period) and precludes analysis of functional connectivity. Functional connectivity could be achieved with functional near-infrared spectroscopy (fNIRS) and electroencephalography (EEG) since these can be implemented during real-time walking (Hamacher et al., 2015). These techniques furthermore offer the benefit of not exposing participants to ionizing radiation or strong magnetic fields. However, both fNIRS and EEG are limited by anatomical imprecision, providing only superficial cortical activity and lack insights into midbrain regions and networks (Tenório et al., 2021). While each technique has its strengths, all modalities face challenges in directly probing for brainstem networks. The intricate anatomical and functional nature of the brainstem poses difficulties for detailed exploration across imaging methodologies (Tracey & Iannetti, 2006).

The slow uptake of FDG by the brain from the circulation occurs after 30 min and plateauing (Ginsberg et al., 1988) and provides a way of measuring changes in neuronal glucose metabolism related to activity during that time. By utilising the capacity to measure neuronal metabolism during gait, one landmark FDG-PET study compared walking with lying supine (la Fougère et al., 2010). This however required two separate study visits with resting and walking scans taking place at least

7-days apart. This can substantially increase participant burden; researchers' time; and findings may be influenced by normal biological fluctuations (Chang et al., 1987; Gordon et al., 2017).

To address these limitations, we assessed the feasibility and effectiveness of a novel methodology with a dual-injection paradigm and two static FDG-PET scans in a single session to measure brain metabolic changes during gait. Previous studies have demonstrated the feasibility of extracting meaningful data following repeated injection of radioisotopes (Brooks et al., 1987; Chang et al., 1987). One such study using FDG-PET to measure brain glucose metabolism found similar activation across the brain when participants performed the same neuropsychological task twice with each task preceded by an FDG bolus injection (Chang et al., 1987). The method proposed by Chang and colleagues (1987) was however optimised for using the kinetic model on PET data with a single scan session and not validated if the tasks require participants to leave the scanner and perform tasks outside of it. These and our findings – with a much more challenging methodology requiring participants to perform intensive activity outside the scanner – suggest that a dual-injection paradigm is feasible and findings are biologically valid in our sample. We cannot comment on other populations who may benefit from our paradigm, this is yet to be assessed. We are however confident that this paradigm may benefit those who find it difficult to attend multiple-testing sessions including those with pathology which fluctuates from one day to the next including those with Parkinson's and multiple sclerosis.

Alongside the paradigm, we used a simple dose correction whereby the residual ^{18}F activity from the first injection is removed from the second scan after a decay correction. To compare the images between participants we chose to scale our data to the global mean and two reference regions, the cerebellum and centrum semiovale in white matter. Although findings are comparable between these different reference regions it was clear that the use of the global mean increased the sensitivity of our findings resulting in larger clusters and higher Z-values. This is in line with the work of others (Borghammer et al., 2008).

Ratio normalisation and the choice of a reference region have been a matter of much debate (Borghammer, 2012; Borghammer et al., 2009; López-González et al., 2020). The use of global mean FDG is common (Fox et al., 1988) and especially utilised in patient-based studies (Borghammer, 2012). However, this has been shown to influence results by inflating findings of hypometabolism in subcortical structures in patients (Borghammer et al., 2009). Our choice of using white matter is based on studies showing this to be a relatively unbiased region, especially in studies of ageing (Borghammer et al., 2008). This is also the region used in studies similar to ours (la Fougère et al., 2010). We furthermore carried out analyses of the data without scaling. This resulted in a minimal change in findings notwithstanding reduced strength of statistical significance.

To summarise, for our specific purposes and objectives, PET/MR imaging was employed. Past investigations on the functional neuroanatomy of gait require scans to be acquired in separate study sessions on separate days. Our novel methodology utilising a dual-injection paradigm and a bespoke dose correction has allowed us to probe the neural substrates of gait, minimising participant burden and previous methodological limitations.

5.2. Walking increases energy demands in widespread regions of the brain

Contrasting PET$_{WALK}$ with PET$_{STAND}$ using whole-brain voxel-wise analysis revealed a greater global impression of the neural networks involved in gait and included novel insights. Our findings demonstrated significantly increased glucose metabolism in the cerebellar vermis IV-V area. Upon closer inspection, we noted that this cluster included the fastigial nucleus and the cerebellar locomotor region (CLR). We found increased glucose utilisation in the midbrain, bilaterally, encompassing the midbrain locomotor region (MLR) and the sensorimotor cortex. We also found activations in a large cluster in the thalamus, specifically in

the intralaminar and mediodorsal nuclei, and putamen. Increased glucose metabolism in these regions during walking resonates with previous findings (Jahn et al., 2004, 2008; la Fougère et al., 2010) and provides further corroboration for the functional equivalent of the supraspinal locomotor brain network identified originally in felines and rats (Garcia-Rill, 1986; Shik & Orlovsky, 1976).

The locomotor network includes projections from the cortical regions involved in motor preparation such as the lateral premotor cortex and the supplementary motor area (SMA), in addition to the striatum, subthalamic locomotor region (SLR), MLR and CLR (Jahn et al., 2008a; 2008b; Mori et al., 2001). While this network is relatively preserved in ageing (Zwergal et al., 2012), FDG-PET studies in patients with atypical parkinsonism, which adversely affects gait, have shown that glucose metabolism is reduced in discrete regions of the supraspinal locomotor network (Zwergal et al., 2013). This study furthermore showed that faster walking and longer steps were associated with relatively increased glucose metabolism in the frontal cortex and SLR and reduced metabolism in the motor cortex and CLR. No associations were however seen in healthy controls.

The exact anatomical location of this network in humans and its spatial extent are still a matter of debate. Physiological noise attributed to respiration-related artefacts may curtail strong interpretation of brainstem activation using fMRI (Raj et al., 2001). By a similar token, it is possible that effects of MR sequences run parallel to PET especially those of electromagnetic and thermal nature may impact FDG uptake. However, recent investigations indicate that the effects are negligible and should not have impacted our findings (Shan et al., 2022). Nonetheless, we interpret any increases in the brainstem with caution.

The MLR is located in the midbrain and corresponds to the dorsal part of the pedunculopontine nucleus (PPN) and cuneiform nucleus (CnF), lying on the ventral border of the inferior colliculus (IC) (Grillner & Shik, 1973; Shik & Orlovsky, 1976). The MLR projects to spinal central pattern generators via the ponto-medullary reticular formation (Armstrong, 1988). The SLR is less well defined but is likely situated dorsomedial to the subthalamic nucleus and is part of the lateral hypothalamus (Garcia-Rill, 1986; Takakusaki, 2017). In humans, it has been posited that both SLR and MLR regions are involved in step initiation and gait automaticity (Boyne et al., 2018; Wei et al., 2020). The CLR – possibly regulating gait speed and variability (Boyne et al., 2018; Wei et al., 2020) – is composed of fastigial nucleus [FN] efferent fibers which principally integrate information from proprioceptive, vestibular, and visual systems (Mori et al., 2001). These areas, together with the prefrontal cortex (via cerebro-cerebellar communication systems) and limbic lobe, promote steady-state locomotion (Brooks & Cullen, 2009; Mori et al., 2001). With these anatomical landmarks in mind, we provide an enhanced view of brainstem activation in our study in Fig. 7. This figure illustrates glucose utilisation during walking in various brainstem nuclei and midline cerebellum. Inspection of Fig. 3 shows a cluster with peak coordinates located within the intralaminar thalamus and further including the substantia nigra, red nucleus and brainstem nuclei. The cluster, especially in the right brainstem overlaps with the PPN and CnF (see Fig. 7), corresponding to the MLR. We did not find any increases however in the SLR, which is in line with the findings of others (Jahn et al., 2008a; la Fougère et al., 2010).

In addition to increases in glucose metabolism in the brainstem (replicating previous findings), our novel methodology contrasting glucose utilisation during walking with that during standing elicited greater glucose metabolism in regions important in visual processing (occipital cortex), vestibular function (a cluster extending to posterior parietal operculum and the anterior subcentral gyrus, the parieto-insular vestibular cortex), and regions critical for higher-order cognitive function such as attention (middle, superior frontal cortex) and anticipation-motor integration (mid cingulate). These findings provide a more comprehensive view of how the brain controls walking and have not been reported previously. As such, these findings are in clear contrast to previous findings (la Fougère et al., 2010). The study by la Fougère and colleagues compared real walking to lying supine in healthy older adults. Differences in the control task (standing, lying) and scan acquisition protocols (single session, different days) may explain some of the differences between the present study and previous work (la Fougère et al., 2010). Their study provided a direct comparison of brain activation during real walking using FDG-PET and motor imagery of locomotion using fMRI. Based on their findings, the authors proposed two pathways including an executive 'direct' network findings bypassing
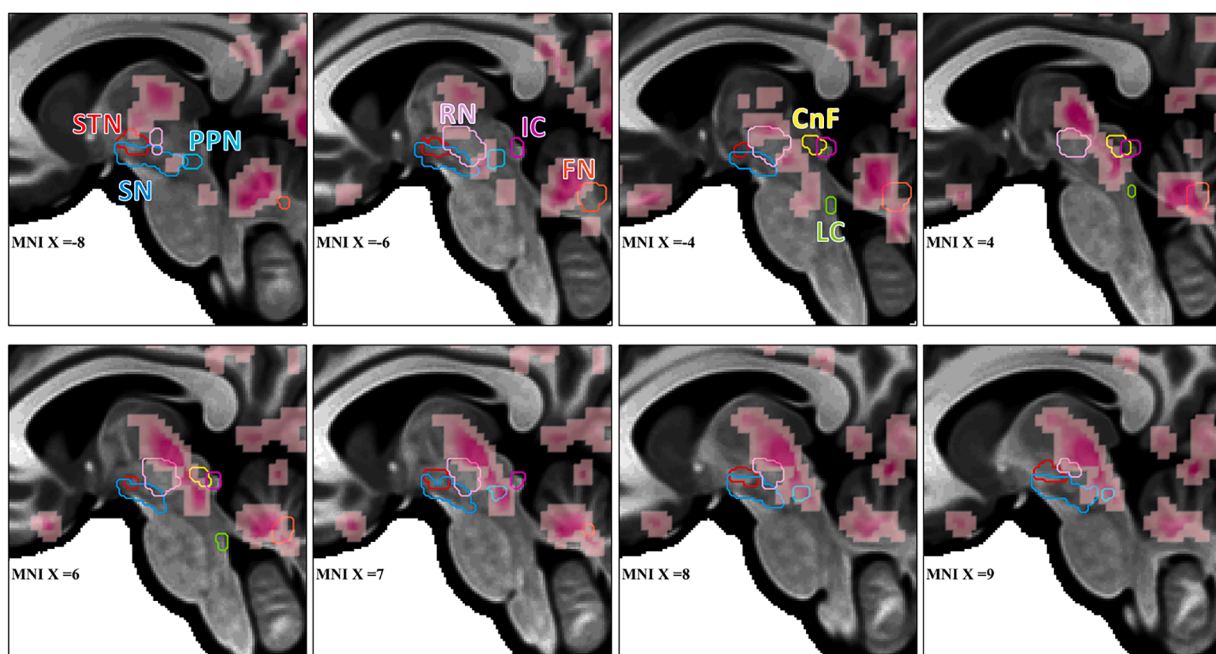

Fig. 7. Enhanced view of brainstem activations during walking relative to standing following proportional scaling using the global mean with contours of brainstem nuclei provided by the BrainstemNavigator atlas (http://www.nitrc.org/projects/brainstemnavig/). The figure is created using the CanlabCore tools (https://github.com/canlab/CanlabCore). Abbreviations: STN – subthalamic nucleus, SN – substantia nigra, PPN – pedunculopontine nucleus, IC – inferior colliculus, CnF – cuneiform nucleus, LC – locus coeruleus, FN – Fastigial nucleus.

subcortical locomotor regions and an 'indirect' more complex planning network (la Fougère et al., 2010). Our findings do not conform to this conclusion since we observed increased neural activity of the brainstem locomotor regions in addition to widespread cortical increases during walking compared with standing. The study by la Fougère et al. (2010) offers supporting evidence that findings from FDG-PET and fMRI measurements of neural activation during walking are similar, albeit with discrete differences observed including greater activation of brainstem nuclei during imagined walking. Unsurprisingly, greater activation of the primary motor cortex was reported following real compared to imagined walking.

Concerning visual processing, this cluster was large (over 16,000 voxels) centered in the cuneus and covering much of Brodmann area 17. Previous neuroimaging studies have shown increased neural activation of this region during mental imagery of steady state walking compared to gait initiation (Malouin et al., 2003). Increased activation of the occipital lobe has been observed during imagined termination of walking and when stepping over obstacles (Wang et al., 2009). This increase in glucose metabolism in the occipital lobe could be due to our protocol. While standing, participants were instructed to fixate on a wall-cross to minimize head movements. Conversely, during the walking task, participants had the freedom to visually explore their surroundings, engaging in a feedforward visual processing approach to plan and execute motor patterns essential for overground walking. We thus posit that when walking, regions of the occipital cortex are recruited to facilitate the processing of visual information, enhance environmental perception and coordinate movements.

We were surprised that our data did not show increased activation of the SMA during walking, suggesting that this region is similarly activated by our control static posture task. It appears that the SMA may be critical in preparing for both static and dynamic postural control which could explain our findings (Ouchi et al., 2001, 1999; Taube et al., 2015). An alternative explanation is that this region is not strongly activated due to the simplicity of our walking condition with participants walking continuously around an oval circuit. Previous imaging studies have observed increased activation of the SMA when the walking task is more challenging with participants navigating through obstacles (van der Meulen et al., 2012). Future studies are needed to address this issue and provide further clarity on the role of the SMA during walking. Our protocol could easily be modified to compare simple and complex walking tasks.

To summarise, our work has revealed that discrete supraspinal locomotor centres are highly active during a walking condition compared to a static postural control task. Our findings of globally increased glucose utilisation in cortical and subcortical regions during walking supports work suggesting locomotion in healthy older adults represents a complex interplay between non-overlapping brain areas that form interactive networks to support successful navigation in the real-world (Wilson et al., 2019).

5.3. Limitations of this study

The results of this study have clearly demonstrated the feasibility of our paradigm to understand the functional neuroanatomy of gait. Although our method localised activity to brain regions with a known function in gait, one limitation of our study is that we did not validate it by comparison against other functional brain imaging techniques. However, a previous study by la Fougère et al. (2010) did demonstrate similar activation patterns during actual walking with FDG-PET compared to simulated walking with fMRI. Our sample size is small with datasets available from 15 participants. However, we do not view this as a major limitation since this was a within-subjects design, which has greater statistical power compared to between-subjects designs. Thus, we view our sample size as large enough to demonstrate the feasibility of the methodology. Our sample of healthy older adults was restricted to those between 60 and 70 years, which may prevent our

findings of the neural substrates of walking being generalisable to younger individuals. Also, in accordance with standardised procedures, we asked our participants to fast for at least 6 h. Approximately 70-min elapsed between injections, making it possible that our findings are influenced by greater uptake in the brain during the second scan (PET$_{WALK}$) since circulating blood glucose levels are lower with less competition for the FDG. We measured blood glucose levels immediately prior to FDG injection and found no statistically significant differences between the two measurements. It has been shown previously that when blood sugar levels are low this may have little to no effects on FDG uptake in the brain (Sarikaya et al., 2019). This indicates that fasting for longer than 6 h (per EANM recommendations Varrone et al., 2009) has negligible effects on brain FDG uptake. This, however, can pose a problem for patient populations who may require sustenance when taking their medication. Another limitation is the possibility of increased muscle uptake during walking, theoretically reducing available brain glucose (Silva-Rodríguez et al., 2017). Both tasks used in the current study impose metabolic demands on the musculoskeletal system to resist the downward acceleration due to gravity. This should be consistent between participants due to the standardized nature of the tasks, and metabolic demands in both would lessen the difference. We see an overall tendency for brain FDG to increase for walking relative to standing, and we would expect reduced glucose availability to globally affect the brain. Yet, we see regional increases in areas relevant to walking.

Finally, we emphasise that the primary aim of this study was to develop a functional methodology to study the neuroanatomy of gait. Although we have reported replicating increased activation of brainstem nuclei, we have done so with great caution and drawn no strong conclusions.

5.4. Conclusions and future work

In conclusion, we have established the feasibility and safety of a novel hybrid FDG-PET paradigm utilising a dual-injection paradigm capturing the neural activity related to real time walking in healthy older adults. We have provided sufficient details in this report for others to employ our paradigm in future works. In addition to furthering the evidence on the existence of the supraspinal locomotor network in humans, we have demonstrated that the functional neuroanatomy of gait using a real-time paradigm includes brain regions important for visual processing, spatial navigation, multi-sensory function, and anticipation-motor integration. Using repeated intravenous injections of FDG within the same scan session and applying our simple methodology we have reduced participant burden, and study time and avoided individual biological day-to-day fluctuations in brain function and network variation that could confound a protocol involving two separate scanning sessions. Future studies are urged to consider these points in a larger sample of participants. We also carried out normalisation of our data to three reference regions and noted strong similarities across all analyses. Other methods, that do not require an *a priori* reference region to be chosen, have been developed. Future studies would need to determine how these approaches impact the data in studies employing paradigms similar to ours.

CRediT authorship contribution statement

Hilmar P. Sigurdsson: Methodology, Formal analysis, Investigation, Resources, Data curation, Writing – original draft, Writing – review & editing, Visualization. **Lisa Alcock:** Conceptualization, Methodology, Investigation, Resources, Writing – original draft, Writing – review & editing, Project administration, Funding acquisition. **Michael Firbank:** Methodology, Validation, Data curation, Writing – original draft, Writing – review & editing. **Ross Wilson:** Formal analysis, Writing – original draft. **Philip Brown:** Conceptualization, Methodology, Investigation. **Ross Maxwell:** Methodology, Validation, Data curation. **Elizabeth Bennett:** Investigation, Resources. **Nicola Pavese:** Conceptualization, Funding acquisition, Supervision, Writing – review & editing. **David J. Brooks:** Conceptualization, Funding acquisition, Supervision, Writing – review & editing. **Lynn Rochester:** Conceptualization, Funding acquisition, Project administration, Supervision, Writing – review & editing.

Declaration of competing interest

Declarations of interest: none. The Funder, GE Healthcare, had no direct intellectual input on the protocol development. The study design, methodology, data analysis and interpretation were independently determined by our research team.

Data availability

Data will be made available on request.

Supplementary materials

Supplementary material associated with this article can be found, in the online version, at doi:10.1016/j.neuroimage.2024.120531.

References

Armstrong, D.M., 1988. The supraspinal control of mammalian locomotion. J. Physiol. 405, 1–37. https://doi.org/10.1113/jphysiol.1988.sp017319.

Axer, H., Axer, M., Sauer, H., Witte, O.W., Hagemann, G., 2010. Falls and gait disorders in geriatric neurology. Clin. Neurol. Neurosurg. 112 (4), 265–274. https://doi.org/10.1016/j.clineuro.2009.12.015.

Baltadjieva, R., Giladi, N., Gruendlinger, L., Peretz, C., Hausdorff, J.M., 2006. Marked alterations in the gait timing and rhythmicity of patients with de novo Parkinson's disease. Eur. J. Neurosci. 24 (6), 1815–1820. https://doi.org/10.1111/j.1460-9568.2006.05033.x.

Beck, A.T., Ward, C.H., Mendelson, M., Mock, J., Erbaugh, J., 1961. An inventory for measuring depression. Arch. Gen. Psychiatry 4, 561–571. https://doi.org/10.1001/archpsyc.1961.01710120031004.

Borghammer, P., 2012. Perfusion and metabolism imaging studies in Parkinson's disease - with special reference to intensity normalization methods. Dan. Med. J. 59 (6), 1–24.

Borghammer, P., Aanerud, J., Gjedde, A., 2009. Data-driven intensity normalization of PET group comparison studies is superior to global mean normalization. Neuroimage 46 (4), 981–988. https://doi.org/10.1016/j.neuroimage.2009.03.021.

Borghammer, P., Cumming, P., Aanerud, J., Gjedde, A., 2009. Artefactual subcortical hyperperfusion in PET studies normalized to global mean: lessons from Parkinson's disease. Neuroimage 45 (2), 249–257. https://doi.org/10.1016/j.neuroimage.2008.07.042.

Borghammer, P., Jonsdottir, K.Y., Cumming, P., Ostergaard, K., Vang, K., Ashkanian, M., Vafaee, M., Iversen, P., Gjedde, A., 2008. Normalization in PET group comparison studies—the importance of a valid reference region. Neuroimage 40 (2), 529–540. https://doi.org/10.1016/j.neuroimage.2007.12.057.

Boyne, P., Maloney, T., DiFrancesco, M., Fox, M.D., Awosika, O., Aggarwal, P., Woeste, J., Jaroch, L., Braswell, D., Vannest, J., 2018. Resting-state functional connectivity of subcortical locomotor centers explains variance in walking capacity. Hum. Brain Mapp. 39 (12), 4831–4843. https://doi.org/10.1002/hbm.24326.

Brooks, J.X., Cullen, K.E., 2009. Multimodal integration in rostral fastigial nucleus provides an estimate of body movement. J. Neurosci. 29 (34), 10499–10511. https://doi.org/10.1523/JNEUROSCI.1937-09.2009.

Brooks, R.A., Dichiro, G., Zukerberg, B.W., Bairamian, D., Larson, S.M., 1987. Test-retest studies of cerebral glucose-metabolism using fluorine-18 deoxyglucose: validation of method. J. Nucl. Med. 28 (1), 53–59.

Bürki, C.N., Bridenbaugh, S.A., Reinhardt, J., Stippich, C., Kressig, R.W., Blatow, M., 2017. Imaging gait analysis: an fMRI dual task study. Brain Behav. 7 (8), e00724. https://doi.org/10.1002/brb3.724.

Chang, J.Y., Duara, R., Barker, W., Apicella, A., Finn, R., 1987. Two behavioral states studied in a single PET/FDG procedure: theory, method, and preliminary results. J. Nucl. Med. 28 (5), 852–860.

Del Din, S., Godfrey, A., Rochester, L., 2016. Validation of an accelerometer to quantify a comprehensive battery of gait characteristics in healthy older adults and Parkinson's disease: toward clinical and at home use. IEEE J. Biomed. Health Inform. 20 (3), 838–847. https://doi.org/10.1109/JBHI.2015.2419317.

Folstein, M.F., Folstein, S.E., McHugh, P.R., 1975. "Mini-mental state". A practical method for grading the cognitive state of patients for the clinician. J. Psychiatr. Res. 12 (3), 189–198. https://doi.org/10.1016/0022-3956(75)90026-6.

Fox, P.T., Raichle, M.E., Mintun, M.A., Dence, C., 1988. Nonoxidative glucose consumption during focal physiologic neural activity. Science (1979) 241 (4864), 462–464. https://doi.org/10.1126/science.3260686.

Garcia-Rill, E., 1986. The basal ganglia and the locomotor regions. Brain Res. Rev. 11 (1), 47–63. https://doi.org/10.1016/0165-0173(86)90009-3.

Ginsberg, M.D., Chang, J.Y., Kelley, R.E., Yoshii, F., Barker, W.W., Ingenito, G., Boothe, T.E., 1988. Increases in both cerebral glucose-utilization and blood-flow during execution of a somatosensory task. Ann. Neurol. 23 (2), 152–160. https://doi.org/10.1002/ana.410230208.

Gordon, E.M., Laumann, T.O., Gilmore, A.W., Newbold, D.J., Greene, D.J., Berg, J.J., Ortega, M., Hoyt-Drazen, C., Gratton, C., Sun, H.X., Hampton, J.M., Coalson, R.S., Nguyen, A.L., McDermott, K.B., Shimony, J.S., Snyder, A.Z., Schlaggar, B.L., Petersen, S.E., Nelson, S.M., Dosenbach, N.U.F., 2017. Precision functional mapping of individual human brains. Neuron 95 (4). https://doi.org/10.1016/j.neuron.2017.07.011, 791-807.e797.

Gribbin, J., Hubbard, R., Smith, C., Gladman, J., Lewis, S., 2009. Incidence and mortality of falls amongst older people in primary care in the United Kingdom. QJM. 102 (7), 477–483. https://doi.org/10.1093/qjmed/hcp064.

Grillner, S., Shik, M.L., 1973. On the descending control of the lumbosacral spinal cord from the "Mesencephalic locomotor region". Acta Physiol. Scand. 87, 320–333. https://doi.org/10.1111/j.1748-1716.1973.tb05396.x.

Hamacher, D., Herold, F., Wiegel, P., Hamacher, D., Schega, L., 2015. Brain activity during walking: a systematic review. Neurosci. Biobehav. Rev. 57, 310–327. https://doi.org/10.1016/j.neubiorev.2015.08.002.

Hammers, A., Allom, R., Koepp, M.J., Free, S.L., Myers, R., Lemieux, L., Mitchell, T.N., Brooks, D.J., Duncan, J.S., 2003. Three-dimensional maximum probability atlas of the human brain, with particular reference to the temporal lobe. Hum. Brain Mapp. 19 (4), 224–247. https://doi.org/10.1002/hbm.10123.

Hétu, S., Grégoire, M., Saimpont, A., Coll, M.P., Eugène, F., Michon, P.E., Jackson, P.L., 2013. The neural network of motor imagery: an ALE meta-analysis. Neurosci. Biobehav. Rev. 37 (5), 930–949. https://doi.org/10.1016/j.neubiorev.2013.03.017.

Jaeger, L., Marchal-Crespo, L., Wolf, P., Riener, R., Michels, L., Kollias, S., 2014. Brain activation associated with active and passive lower limb stepping. Front. Hum. Neurosci. 8, 828. https://doi.org/10.3389/fnhum.2014.00828.

Jahn, K., Deutschländer, A., Stephan, T., Kalla, R., Hüfner, K., Wagner, J., Strupp, M., Brandt, T., 2008a. Supraspinal locomotor control in quadrupeds and humans. In: Proceedings of the *Using Eye Movements as an Experimental Probe of Brain Function - a Symposium in Honor of Jean Buttner-Ennever*, 171, pp. 353–362. https://doi.org/10.1016/S0079-6123(08)00652-3.

Jahn, K., Deutschlander, A., Stephan, T., Kalla, R., Wiesmann, M., Strupp, M., Brandt, T., 2008b. Imaging human supraspinal locomotor centers in brainstem and cerebellum. Neuroimage 39 (2), 786–792. https://doi.org/10.1016/j.neuroimage.2007.09.047.

Jahn, K., Deutschlander, A., Stephan, T., Strupp, M., Wiesmann, M., Brandt, T., 2004. Brain activation patterns during imagined stance and locomotion in functional magnetic resonance imaging. Neuroimage 22 (4), 1722–1731. https://doi.org/10.1016/j.neuroimage.2004.05.017.

la Fougère, C., Zwergal, A., Rominger, A., Forster, S., Fesl, G., Dieterich, M., Brandt, T., Strupp, M., Bartenstein, P., Jahn, K., 2010. Real versus imagined locomotion: a [18F]-FDG PET-fMRI comparison. Neuroimage 50 (4), 1589–1598. https://doi.org/10.1016/j.neuroimage.2009.12.060.

Levy-Cooperman, N., Ramirez, J., Lobaugh, N.J., Black, S.E., 2008. Misclassified tissue volumes in Alzheimer disease patients with white matter hyperintensities - importance of lesion segmentation procedures for volumetric analysis. Stroke 39 (4), 1134–1141. https://doi.org/10.1161/Strokeaha.107.498196.

López-González, F.J., Silva-Rodríguez, J., Paredes-Pacheco, J., Niñerola-Baizán, A., Efthimiou, N., Martín-Martín, C., Moscoso, A., Ruibal, Á., Roé-Vellvé, N., Aguiar, P., 2020. Intensity normalization methods in brain FDG-PET quantification. Neuroimage 222. https://doi.org/10.1016/j.neuroimage.2020.117229.

Malouin, F., Richards, C.L., Jackson, P.L., Dumas, F., Doyon, J., 2003. Brain activations during motor imagery of locomotor-related tasks: A PET study. Human brain mapping 19 (1), 47–62.

Mori, S., Matsuyama, K., Mori, F., Nakajima, K., 2001. Supraspinal sites that induce locomotion in the vertebrate central nervous system. Adv. Neurol. 87, 25–40.

Ouchi, Y., Okada, H., Yoshikawa, E., Furatsubashi, M., Nobezawa, S., 2001. Absolute changes in regional cerebral blood flow in association with upright posture in humans: An orthostatic PET study. J. Nucl. Med. 42 (5), 707–712.

Ouchi, Y., Okada, H., Yoshikawa, E., Nobezawa, S., Futatsubashi, M., 1999. Brain activation during maintenance of standing postures in humans. Brain 122, 329–338. https://doi.org/10.1093/brain/122.2.329.

Personnier, P., Kubicki, A., Laroche, D., Papaxanthis, C., 2010. Temporal features of imagined locomotion in normal aging. Neurosci. Lett. 476 (3), 146–149. https://doi.org/10.1016/j.neulet.2010.04.017.

Pickett, K.A., Peterson, D.S., Earhart, G.M., 2012. Motor imagery of gait tasks in individuals with Parkinson disease. J. Parkinsons. Dis. 2 (1), 19–22. https://doi.org/10.3233/JPD-2012-11045.

Raj, D., Anderson, A.W., Gore, J.C., 2001. Respiratory effects in human functional magnetic resonance imaging due to bulk susceptibility changes. Phys. Med. Biol. 46 (12), 3331–3340. https://doi.org/10.1088/0031-9155/46/12/318.

Reivich, M., Kuhl, D., Wolf, A., Greenberg, J., Phelps, M., Ido, T., Casella, V., Fowler, J., Hoffman, E., Alavi, A., Som, P., Sokoloff, L., 1979. The [^{18}F]fluorodeoxyglucose method for the measurement of local cerebral glucose utilization in man. Circ. Res. 44 (1), 127–137. https://doi.org/10.1161/01.res.44.1.127.

Rolls, E.T., Huang, C.C., Lin, C.P., Feng, J.F., Joliot, M., 2020. Automated anatomical labelling atlas 3. Neuroimage 206. https://doi.org/10.1016/j.neuroimage.2019.116189.

Sarikaya, I., Sarikaya, A., Sharma, P., 2019. Assessing the effect of various blood glucose levels on F-FDG activity in the brain, liver, and blood pool. J. Nucl. Med. Technol. 47 (4), 313–318. https://doi.org/10.2967/jnmt.119.226969.

Schmidt, P., Gaser, C., Arsic, M., Buck, D., Förschler, A., Berthele, A., Hoshi, M., Ilg, R., Schmid, V.J., Zimmer, C., Hemmer, B., Mühlau, M., 2012. An automated tool for detection of FLAIR-hyperintense white-matter lesions in multiple sclerosis. Neuroimage 59 (4), 3774–3783. https://doi.org/10.1016/j.neuroimage.2011.11.032.

Schwarz, C.G., Gunter, J.L., Ward, C.P., Kantarci, K., Senjem, M.L., Petersen, R.C., Knopman, D.S., Jack, C.R., 2018. P3-382: methods to improve Spm12 tissue segmentations of older adult brains. Alzheimer's & Dementia 14 (7S_Part_23). https://doi.org/10.1016/j.jalz.2018.06.1744.

Shan, Y., Wang, Z., Song, S.S., Xue, Q.Y., Ge, Q., Yang, H.W., Cui, B.X., Zhang, M., Zhou, Y., Lu, J., 2022. Integrated positron emission tomography/magnetic resonance imaging for resting-state functional and metabolic imaging in human brain: what is correlated and what is impacted. Front. Neurosci. 16 https://doi.org/10.3389/fnins.2022.824152.

Shik, M.L., Orlovsky, G.N., 1976. Neurophysiology of locomotor automatism. Physiol. Rev. 56 (3), 465–501. https://doi.org/10.1152/physrev.1976.56.3.465.

Sigurdsson, H.P., Yarnall, A.J., Galna, B., Lord, S., Alcock, L., Lawson, R.A., Colloby, S.J., Firbank, M.J., Taylor, J.P., Pavese, N., Brooks, D.J., O'Brien, J.T., Burn, D.J., Rochester, L., 2022. Gait-related metabolic covariance networks at rest in Parkinson's disease. Mov. Disord. 37 (6), 1222–1234. https://doi.org/10.1002/mds.28977.

Silva-Rodríguez, J., Domínguez-Prado, I., Pardo-Montero, J., Ruibal, A.A., Aguiar, P., 2017. Impact of muscular uptake and statistical noise on tumor quantification based on simulated FDG-PET studies. Radiat. Phys. Chem. 131, 28–34. https://doi.org/10.1016/j.radphyschem.2016.10.015.

Takakusaki, K., 2017. Functional neuroanatomy for posture and gait control. J. Mov. Disord. 10 (1), 1–17. https://doi.org/10.14802/jmd.16062.

Taube, W., Mouthon, M., Leukel, C., Hoogewoud, H.M., Annoni, J.M., Keller, M., 2015. Brain activity during observation and motor imagery of different balance tasks: an fMRI study. Cortex 64, 102–114. https://doi.org/10.1016/j.cortex.2014.09.022.

Tenório, K., Pereira, E., Remigio, S., Costa, D., Oliveira, W., Dermeval, D., da Silva, A.P., Bittencourt, I.I., Marques, L.B., 2021. Brain-imaging techniques in educational technologies: a systematic literature review. Educ. Inf. Technol. (Dordr) 27 (1), 1183–1212. https://doi.org/10.1007/s10639-021-10608-x.

Tracey, I., Iannetti, G.D., 2006. Brainstem functional imaging in humans. Suppl. Clin. Neurophysiol. 58, 52–67. https://doi.org/10.1016/s1567-424x(09)70059-5.

van der Meulen, M., Allali, G., Rieger, S.W., Assal, F., Vuilleumier, P., 2012. The influence of individual motor imagery ability on cerebral recruitment during gait imagery. Hum. Brain Mapp. 35 (2), 455–470. https://doi.org/10.1002/hbm.22192.

Varrone, A., Asenbaum, S., Vander Borght, T., Booij, J., Nobili, F., Någren, K., Darcourt, J., Kapucu, Ö.L., Tatsch, K., Bartenstein, P., Van Laere, K., 2009. EANM procedure guidelines for PET brain imaging using [^{18}F]FDG, version 2. Eur. J. Nucl. Med. Mol. ImAging 36 (12), 2103–2110. https://doi.org/10.1007/s00259-009-1264-0.

von Schulthess, G.K., Schlemmer, H.P., 2009. A look ahead: PET/MR versus PET/CT. Eur. J. Nucl. Med. Mol. ImAging 36, S3–S9. https://doi.org/10.1007/s00259-008-0940-9.

Wang, J., Wai, Y., Weng, Y., Ng, K., Huang, Y.Z., Ying, L., Liu, H., Wang, C., 2009. Functional MRI in the assessment of cortical activation during gait-related imaginary tasks. Journal of neural transmission 116, 1087–1092.

Wei, P., Zou, T., Lv, Z., Fan, Y., 2020. Functional MRI Reveals Locomotion-Control Neural Circuits in Human Brainstem. Brain Sci. 10 (10) https://doi.org/10.3390/brainsci10100757.

Wilson, J., Alcock, L., Yarnall, A.J., Lord, S., Lawson, R.A., Morris, R., Taylor, J.P., Burn, D.J., Rochester, L., Galna, B., 2020. Gait progression over 6 years in Parkinson's disease: effects of age, medication, and pathology. Front. Aging Neurosci. 12, 577435 https://doi.org/10.3389/fnagi.2020.577435.

Wilson, J., Allcock, L., Mc Ardle, R., Taylor, J.P., Rochester, L., 2019. The neural correlates of discrete gait characteristics in ageing: a structured review. Neurosci. Biobehav. Rev. 100, 344–369. https://doi.org/10.1016/j.neubiorev.2018.12.017.

Zwergal, A., la Fougère, C., Lorenzl, S., Rominger, A., Xiong, G.M., Deutschenbaur, L., Schöberl, F., Linn, J., Dieterich, M., Brandt, T., Strupp, M., Bartenstein, P., Jahn, K., 2013. Functional disturbance of the locomotor network in progressive supranuclear palsy. Neurology 80 (7), 634–641. https://doi.org/10.1212/WNL.0b013e318281cc43.

Zwergal, A., Linn, J., Xiong, G., Brandt, T., Strupp, M., Jahn, K., 2012. Aging of human supraspinal locomotor and postural control in fMRI. Neurobiol. Aging 33 (6), 1073–1084. https://doi.org/10.1016/j.neurobiolaging.2010.09.022.